CARBON 50 (2012) 3836–3844

Available at www.sciencedirect.com

SciVerse ScienceDirect

journal homepage: www.elsevier.com/locate/carbon

In situ transmission electron microscopy of electrochemical lithiation, delithiation and deformation of individual graphene nanoribbons

Xiao Hua Liu [a], *Jiang Wei Wang* [b], *Yang Liu* [a], *He Zheng* [b,g], *Akihiro Kushima* [c], *Shan Huang* [d], *Ting Zhu* [d], *Scott X. Mao* [b], *Ju Li* [c], *Sulin Zhang* [e], *Wei Lu* [f], *James M. Tour* [f], *Jian Yu Huang* [a,*]

[a] *Center for Integrated Nanotechnologies (CINT), Sandia National Laboratories, Albuquerque, NM 87185, USA*
[b] *Department of Mechanical Engineering and Materials Science, University of Pittsburgh, Pittsburgh, PA 15261, USA*
[c] *Department of Nuclear Science and Engineering and Department of Materials Science and Engineering, Massachusetts Institute of Technology, Cambridge, MA 02139, USA*
[d] *Woodruff School of Mechanical Engineering, Georgia Institute of Technology, Atlanta, GA 30332, USA*
[e] *Department of Engineering Science and Mechanics, Pennsylvania State University, University Park, PA 16802, USA*
[f] *Department of Chemistry, Department of Mechanical Engineering and Materials Science, and The Smalley Institute for Nanoscale Science and Technology, Rice University, Houston, TX 77005, USA*
[g] *School of Physics and Technology, Center for Electron Microscopy and MOE Key Laboratory of Artificial Micro- and Nano-structures, Wuhan University, Wuhan 430072, People's Republic of China*

ARTICLE INFO

Article history:
Received 15 January 2012
Accepted 5 April 2012
Available online 13 April 2012

ABSTRACT

We report an *in situ* transmission electron microscopy study of the electrochemical behavior of few-layer graphene nanoribbons (GNRs) synthesized by longitudinal splitting the multi-walled carbon nanotubes (MWCNTs). Upon lithiation, the GNRs were covered by a nanocrystalline lithium oxide layer attached to the surfaces and edges of the GNRs, most of which were removed upon delithiation, indicating that the lithiation/delithiation processes occurred predominantly at the surfaces of GNRs. The lithiated GNRs were mechanically robust during the tension and compression tests, in sharp contrast to the easy and brittle fracture of the lithiated MWCNTs. This difference is attributed to the unconfined stacking of planar carbon layers in GNRs leading to a weak coupling between the intralayer and interlayer deformations, as opposed to the cylindrically confined carbon nanotubes where the interlayer lithium produces large tensile hoop stresses within the circumferentially-closed carbon layers, causing the ease of brittle fracture. These results suggest substantial promise of graphene for building durable batteries.

© 2012 Elsevier Ltd. All rights reserved.

1. Introduction

Graphene, a monolayer of honeycomb lattice of sp^2-bonded carbon [1], has attracted considerable attention due to its unique structure and properties, and potential applications in many fields including nanoelectronics, photovoltaics, sensors, and renewable energy harvest/storage [2]. As a new material, graphene has the following exceptional merits: (1) It has a vast specific surface area of 2630 m^2/g [3], much larger than that of graphite (~10 m^2/g) or single-walled carbon

* *Corresponding author:* Fax: +1 505 284 7778.
E-mail address: jhuang@sandia.gov (J.Y. Huang).
0008-6223/$ - see front matter © 2012 Elsevier Ltd. All rights reserved.
http://dx.doi.org/10.1016/j.carbon.2012.04.025

nanotubes (SWCNTs, ~1315 m^2/g) [2,4]. (2) It has high electrical conductivity of ~80000 S/m [5], which is about 60 times higher than that of SWCNTs [4]. (3) It is extremely flexible due to the two-dimensional nature and the strong in-plane bonding [6]. As an anode material for lithium ion batteries (LIBs), graphene alone has exhibited high capacities in the range of 540–1264 mAh/g depending on the fabrication and testing methods [4], and there are many ongoing attempts to improve the performance by compositing with other high-capacity materials (Si [7], S [8], SnO_2 [9], etc.) or minimizing restacking with spacer materials (CNTs, C_{60} molecules, etc.) [10].

Although graphene is known for its remarkably high stability in its native state, little is known about the lithiation/delithiation mechanisms and its mechanical stability after lithiation. Degradation of electrode materials often occurs due to the complex electrochemical and mechanical interactions during the lithiation/delithiation cycles. For instance, arc-discharged multi-walled carbon nanotubes (MWCNTs) with few defects are known as a strong material with the Young's modulus up to 1 TPa and the tensile strength about 100 GPa [11], however, they undergo brittle fracture after lithiation as revealed by *in situ* transmission electron microscopy (TEM) [12]. Conventional electrochemical tests also confirmed the breakage of the MWCNTs grown by the chemical vapor deposition (CVD) method after long cycles [13]. These results indicate that despite CNTs' exceptional mechanical strength and their seemingly small intertubular spacing change of only 5.9% after lithiation [12], they are significantly weakened during battery operation. A natural question arises: is similar embrittlement also occurring in graphene upon lithiation? To answer this question, we conducted *in situ* electrochemical and mechanical tests on graphene nanoribbons (GNRs, with about 5–8 layers of graphene sheets [5]) in a nanoscale all-solid electrochemical cell ("solid cell") inside a TEM [14–16]. We found that lithiation/delithiation occurred mainly on the graphene surface, and the lithiated GNRs were mechanically robust and stable, and never showed brittle fracture as seen in the MWCNTs. Actually, the GNRs exhibited great flexibility in the tension and compression tests after lithiation. These results demonstrate the potential of using graphene as a promising candidate for anode or compositing agent in LIBs.

2. Experimental

2.1. *In situ* TEM experiments

The GNRs were produced by longitudinal splitting of MWCNTs reported elsewhere [5]. The as-prepared GNRs have few defects as indicated by their high conductivity measured to be on the order of 80000 S/m, which is close to that of mechanically exfoliated graphene from graphite [5]. The nano-battery was constructed for the *in situ* lithiation experiments using the Nanofactory® TEM-scanning tunneling microscopy (STM) holder [12,14–22]. Briefly, the GNRs were glued to an Al rod with the conductive epoxy (CircuitWorks® Conductive Epoxy, Chemtronics®, Inc.) [12]. Bulk lithium metal was scratched from a Li foil with a tungsten rod inside a glove box (Unilab Glovebox System, MBraun Inc.) filled with helium (both water and oxygen concentrations below 1 ppm). The Li metal served as the Li source and reference electrode. During the sample loading process, the average exposure time to the air was less than 2 s, and a Li_2O layer grew on the surface of the Li metal, which served as the solid electrolyte for Li^+ transport [14,15]. Because the glove box was purged with high-purity helium, the nitrogen concentration was extremely low and no nitride or nitrate formation was found in TEM characterizations. The Li_2O/Li electrode on the mobile STM probe was driven to contact one suspending GNR. A potential of −2 V was applied to the GNR with respect to the Li counter electrode to initiate the lithiation, while the bias was reversed to facilitate delithiation.

Fig 1a shows the schematic illustration of the solid cell: the GNR and Li metal are the two electrodes [12], while a naturally-grown Li_2O layer is the solid electrolyte [14–16]. To avoid possible electron beam effects (such as radiolysis or sputtering damage of both the Li-containing species and the graphene lattice) [23], the TEM was operated at 100 kV and the beam intensity was minimized (~10^{-3} A/cm^2).

2.2. *Ab initio modeling*

To evaluate the lithiation effect on the mechanical property of graphene, we performed *ab initio* simulations of graphene and graphite under tension using the Vienna *Ab Initio* Simulation Package (VASP) [24,25]. A $8.51 \times 7.37 \times 10.0$ Å unit cell including 24 carbon atoms was used for the calculation of the graphene; *x and*, *y* directions correspond to the zigzag and the armchair directions, respectively. We employed density functional theory formalism with generalized gradient approximation parameterized by Perdew and Wang using plane wave basis set [26]. The ionic cores were represented with projector-augmented wave potentials [27,28]. An energy cutoff of 350 eV was chosen for the expansion of the plane wave function and a $8 \times 8 \times 1$ Monkhorst–Pack [29] ***k***-point mesh was selected in the simulations. First, the atomic configurations and the cell vectors were relaxed to minimize the total energy of the graphene system. Then the tensile strain was applied to the model by elongating the simulation cell along *x* (zigzag) direction with the increment of 0.01. After the each increment of the strain, the structural optimization was performed while fixing the cell size in *x* and *z* directions. The same procedure was applied to simulate the tension along *y* (armchair) direction (the structure was optimized while fixing the cell size in *y* and *z* directions after the each strain increment along *y*). The 4 Li atoms were placed uniformly on top of the graphene and the structural optimization was performed to create the C_6Li graphene model. Then, the tensile simulation was conducted following the procedure described above. For the lithiated graphite, a $8.61 \times 7.45 \times 3.45$ Å unit cell including 24 C and 4 Li atoms was used. $8 \times 8 \times 16$ Monkhorst–Pack [29] ***k***-point mesh was selected in the simulations. The cell size was relaxed in *z* direction during tension. All other conditions were the same as the graphene calculation.

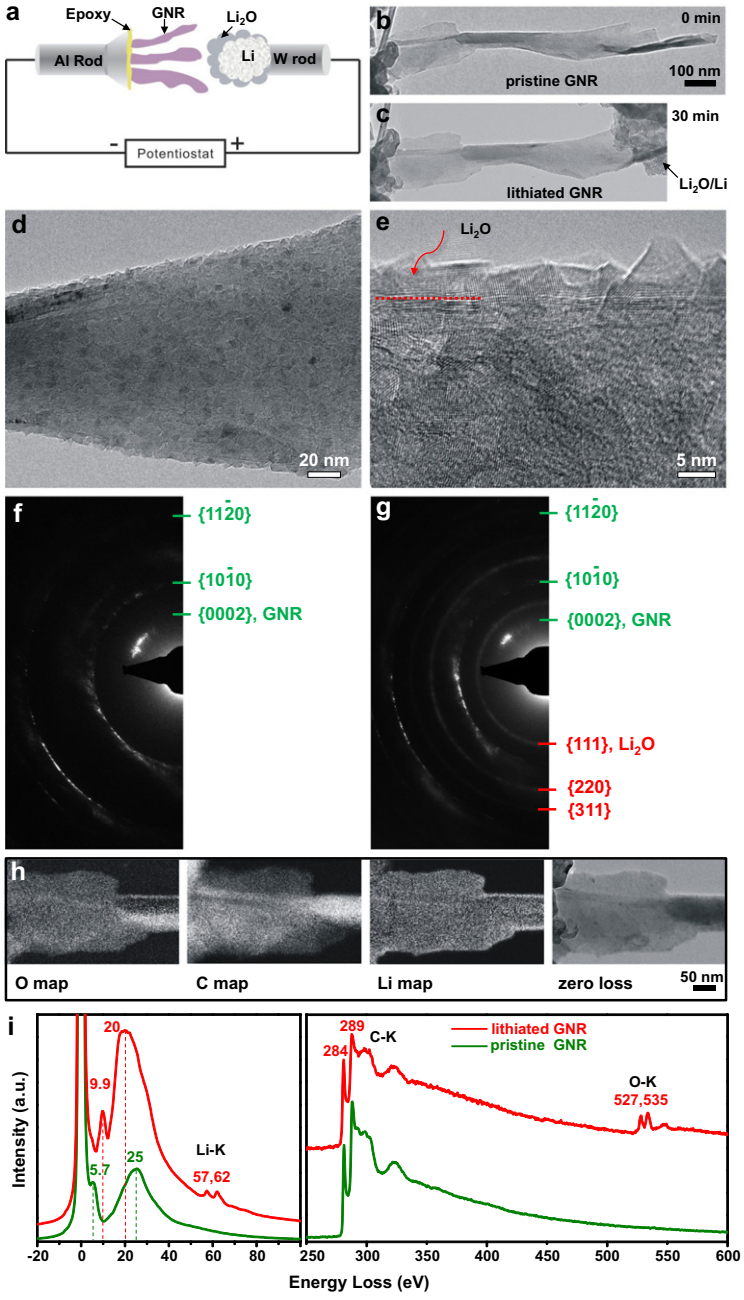

Fig. 1 – Electrochemical lithiation of a graphene nanoribbon (GNR). (a) Schematic illustration of the *in situ* TEM electrochemical experiment setup. The GNRs are glued to the Al rod with conductive epoxy, and Li metal on the W probe is the other electrode. The native Li_2O layer on the Li metal is the solid electrolyte for Li^+ transport. A negative bias is applied to the GNR terminal to initiate lithiation. (b) Pristine GNR. (c) Lithiated GNR with the Li_2O/Li electrode contacting the free end. (d and e) High magnification images showing the lithiated GNR covered by a uniform Li_2O layer. The red dash line marks the profile of the bent GNR (e), and the Li_2O layer is about 5 nm thick with faceted crystallites. (f and g) Electron diffraction patterns (EDPs) from the pristine (f) and lithiated GNR (g). The diffraction rings of {0002} plane indicated that the spacing between the graphene layers increased from 3.4 to 3.6 Å after lithiation, while the diffraction rings from the $\{10\bar{1}0\}$ and $\{11\bar{2}0\}$ planes remained unchanged. Three rings from the polycrystalline Li_2O coating appeared in the lithiated GNR. (h) Electron energy loss spectroscopy (EELS) mapping showing the distribution of O, C, and Li along with the zero loss image. (i) EELS spectra of the pristine and lithiated GNR. The pristine GNR showed well-defined C–K edge with sharp peaks at 284 eV corresponding to the 1s to π^* excitation and 289 eV corresponding to the 1s $\rightarrow$ σ^* excitation, and no oxygen peaks were observed. After lithiation, Li–K (onset at 57 eV) and O–K (onset at 527 eV) appeared, and change of the low loss peaks was obvious (from 5.7 and 25 eV to 9.9 and 20 eV due to the Li_2O attachment), consistent with the EDP and TEM images showing the Li_2O-wrapped GNR.

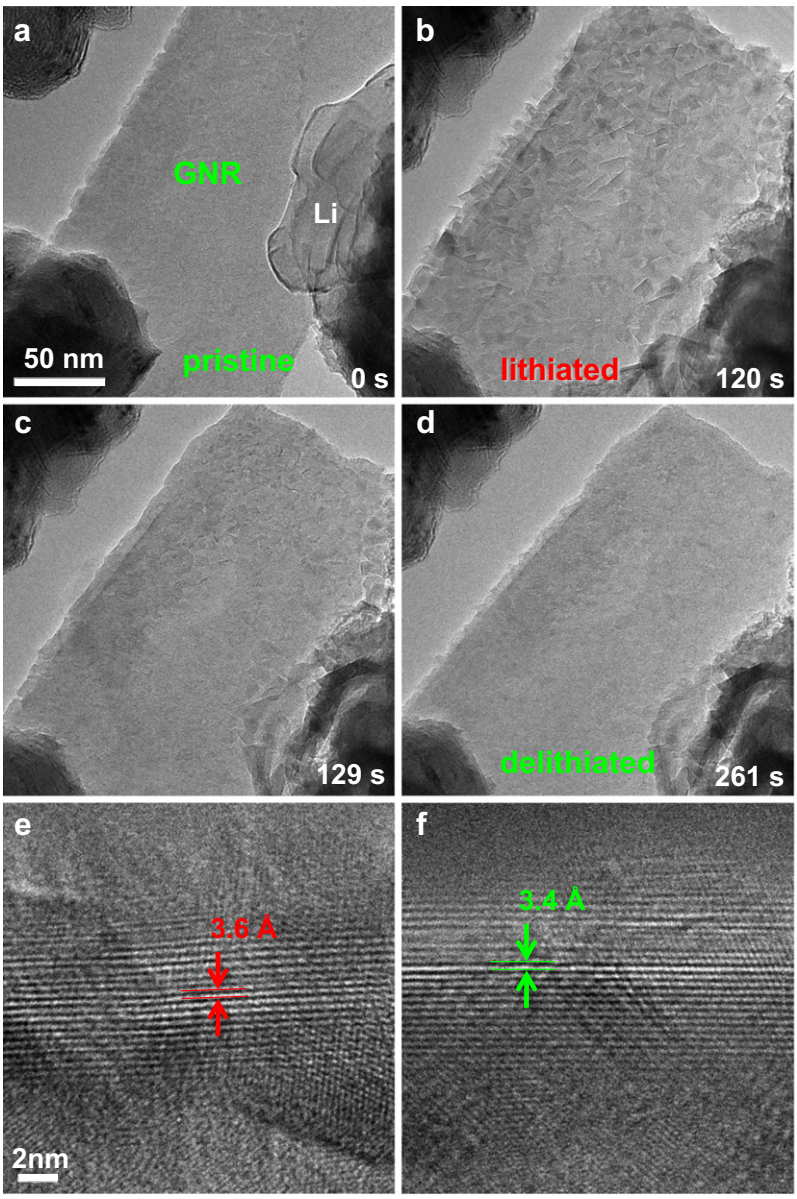

Fig. 2 – Morphology evolution in the sequential lithiation and delithiation processes of a GNR. (a) Pristine GNR. (b) Lithiated GNR with a rough surface decorated with Li_2O crystallites. (c and d) Morphology evolution of the GNR during delithiation. The Li_2O crystallites disappeared (d), and the uniform contrast was similar to the starting state shown in (a), but actually a thin Li_2O layer was left. (e and f) High magnification images showing the interlayer spacing shrank from 3.6 Å of the lithiated state (e) to 3.4 Å of the delithiated state (f).

3. Results and discussion

3.1. *Electrochemical lithiation and delithiation of GNRs*

Fig. 1b shows a pristine GNR stack (5–8 layers) with the length about 1 μm. After the GNR contacted the Li_2O layer, a potential of −2 V was applied between the GNR and the Li metal electrodes. Fig. 1c shows the morphology of the GNR after 30 min of lithiation. Close-up images show that the surface of the GNR was coated by a uniform layer of triangular crystallites (Fig. 1d and e), which was about 5 nm thick and was identified to be Li_2O by comparing the electron diffraction patterns (EDPs) from the pristine (Fig. 1f) and lithiated GNR (Fig. 1g). The (1 1 1) plane of the Li_2O nanocrystals with the lattice spacing of 2.67 Å was resolved on the surface of the GNR after lithiation (Fig. 1e). The d-spacing of the few-layer GNR (0 0 0 2) plane was increased from 3.35 to 3.59 Å after lithiation (Fig. 1f and g), corresponding to a 7.2% expansion induced by lithium intercalation into the graphene layers, while the 2.13 Å spacing of the $(10\bar{1}0)$ plane remained unchanged. Fig. 1h displays the elemental maps (O, C, Li) along with the zero loss image by energy-filtered transmission electron microscopy (EFTEM), showing that Li_2O covered the entire GNR and being consistent with the high resolution images (Fig. 1d and e). The electron energy loss spectroscopy (EELS) spectra of the pristine GNR

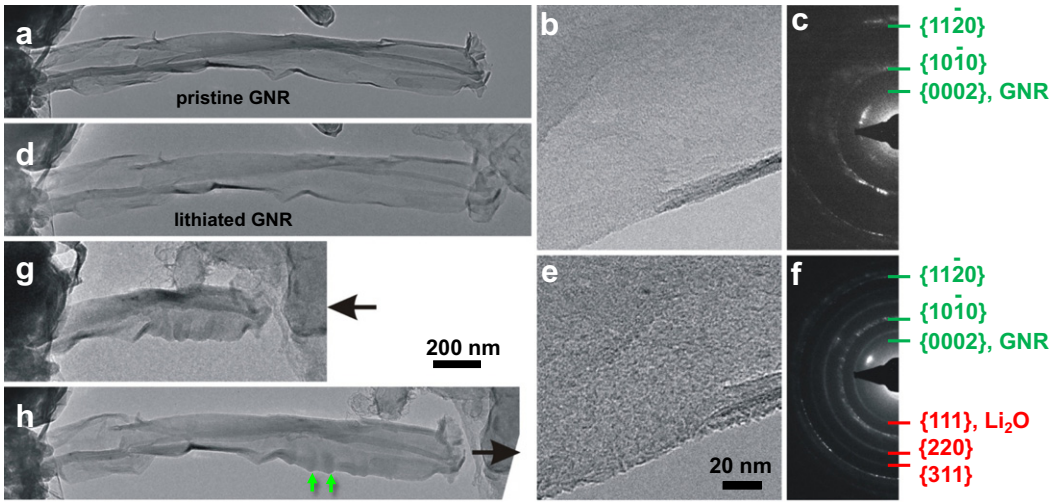

Fig. 3 – Mechanical test of a lithiated GNR. (a–c) Pristine GNR. The GNR was about 1200 nm long and 200 nm wide (a), with a clean surface (b) and crystalline nature as revealed by the EDP (c). (d–f) Lithiated GNR. While the low magnification image did not show much difference (d), the high magnification image (e) and the EDP (f) revealed a Li_2O-coated GNR structure with expanded basal planes. (g–h) The GNR was bent and buckled upon compression (g) and almost recovered to the original shape after the mechanical load was removed (h). The green arrows indicate the wrinkles created by the compression, indicating existence of plastic deformation.

(green trace in Fig. 1i) reveal the well-defined C–K edge (onset at 284 eV) and plasmon peaks (5.7 and 25 eV). The peak at 284 eV corresponds to the $1s \rightarrow \pi^*$ excitation and 289 eV to $1s \rightarrow \sigma^*$ excitation of the sp^2-bonded carbon [30,31]. The plasmon peaks at 5.7 and 25 eV from the pristine few-layer GNR correspond to the π^* and $\pi^* + \sigma^*$ modes, respectively, which are expected for the graphene layer number between 5 and 10 [30,31]. The low loss energy of the GNRs was significantly larger than that from a single graphene sheet (4.7 and 14.6 eV) but slightly lower than that of bulk graphite (7 and 26 eV) [31], being consistent with the GNRs longitudinally split from MWCNTs. The well-defined π^* peak (284 eV) of the C–K edge and the lack of the O–K edge (~535 eV) indicate the high purity of the GNR without detectable oxygen. However, the EELS spectrum of the lithiated GNR clearly shows the Li–K and O–K edges (red traces in Fig. 1i), consistent with the EDPs and high resolution images showing the Li_2O-wrapped around the GNR (Fig. 1e and g). The onset energy of the C–K edge was essentially the same for the pristine and lithiated GNR, which is consistent with previous EELS studies on graphite and LiC_6 [32]. We note that significant energy shift of the plasmon peaks to about 9.9 and 20 eV occurred in the lithiated GNR (vertical dash lines in Fig. 1i) which were mainly due to the formation of Li_2O [32]; however, rigorous EELS interpretation for the Li–C interaction will rely on the minimization of material changes during EELS acquisition (such as oxidation of Li by the residual oxygen and moisture in the TEM column [23,32] and beam-induced damage or conversion [23]), which was not possible in the current experiment. Nevertheless, the attachment of Li_2O on graphene sheets is similar to the lithiation behavior of MWCNTs [12], indicating that it is an intrinsic property of the interaction between lithium and exposed graphite basal planes. Compared to other anode materials (Si, Ge, Al, SnO_2, etc.) tested with the same experimental setup, the quick formation of a thick Li_2O layer on CNTs and graphene is probably related to the formation of the solid electrolyte interface (SEI) layer in carbonaceous materials. In the current experimental configuration, the Li_2O formation is likely due to oxidation of the Li atoms attached to the carbon sheets by the residue oxygen in the TEM column. In real batteries, other Li-containing compounds such as carbonates and alkylates could be formed due to the different chemical environments.

To exclude the electron beam irradiation effect during the lithiation process, control experiments were also conducted with the electron beam blanked except for intermittent short time beam exposure for imaging (Fig. S1). Similar to the GNR lithiation behavior under the weak electron beam, the *d*-spacing of the GNR (0002) plane increased from 3.4 to 3.6 Å after lithiation (Fig. S1f and g), and the surface of the GNR was also coated with a uniform Li_2O layer. Fig. 2 shows the lithiation and delithiation process of another GNR (also see Movie S1 in Supporting Information). As the lithiation process proceeded, a Li_2O layer emerged and covered the GNR surface in 2 min (Fig. 2a and b). The delithiation process was initiated by reversing the polarity of the bias (i.e., applying a +2 V bias on the GNR), and the triangular Li_2O crystals gradually shrank (Fig. 2c) and almost disappeared after full delithiation at 261 s (Fig. 2d), which might be caused by the electrochemical induced decomposition of Li_2O. Prolonged delithiation did not lead to detectable changes in morphology or diffraction patterns. The (0002) plane of the GNR decreased from 3.6 to 3.4 Å after delithiation (Fig. 2e and f), indicating the GNR was fully delithiated. However, a thin layer of Li_2O was left on the surface of GNR, which forms the stable SEI layer. The formation of such a thin layer of Li_2O indicates a loss of capacity in the first cycle. The results indicated clearly that the lithiation/delithiation of the GNRs occurred predominantly at its free surfaces.

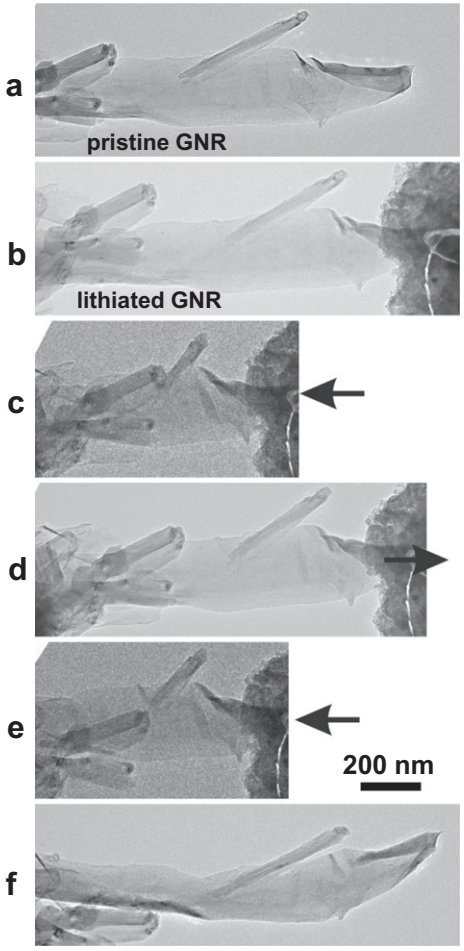

Fig. 4 – Repeated mechanical manipulation of a lithiated GNR. (a) Pristine GNR. (b) Lithiated GNR. (c–f) Morphology change of the lithiated GNR in two compression-release cycles. The GNR showed no obvious change after the mechanical tests (f).

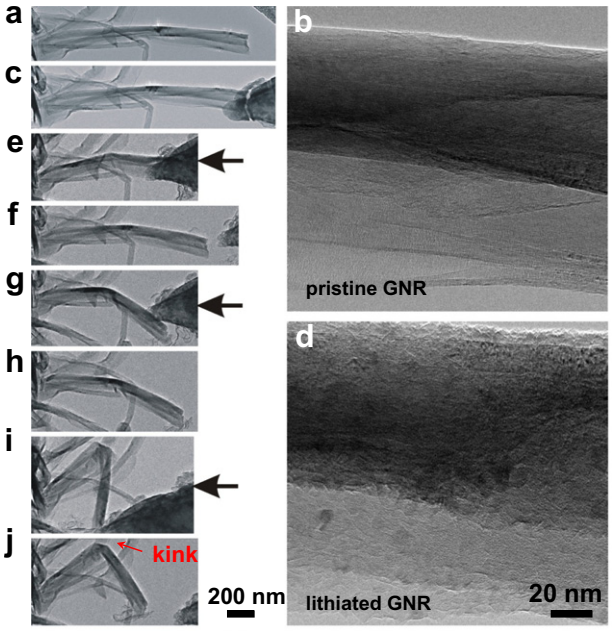

Fig. 5 – Mechanical robustness of a lithiated GNR. (a and b) Pristine GNR. (c and d) Lithiated GNR. (e and j) Morphology change of the lithiated GNR in the three compression-release cycles. Although the lithiated Li_2O/GNR did not return to the straight morphology after mechanical manipulation, neither did it fracture. The red arrow marks the permanent kink formed during the mechanical manipulation.

3.2. *Mechanical robustness of lithiated GNRs*

The mechanical stability of the lithiated GNRs was tested with the tension and compression deformation. Fig. 3 shows the typical lithiation and subsequent deformation process of a GNR. Except for imaging, the electron beam was blocked to minimize the electron beam exposure induced damage to the GNRs during the lithiation process, which may also affect the deformation behavior. Fig. 3a and c present the initial morphologies and EDP of the pristine GNR. The GNR was about 1200 nm long and 150 nm wide, showing a ribbon-like shape. Similar to other lithiated GNRs, a uniform Li_2O layer formed on the GNR surface after 30 min of lithiation (Fig. 3d and e), and the (0002) spacing increased from 3.4 to 3.6 Å (Fig. 3c and f). The lithiated GNR was then compressed by the Li_2O/Li electrode and released (Fig. 3g and h). During the compression, the lithiated GNR gradually bent and buckled (Fig. 3g and Movie S2). Intriguingly, the shape was almost fully recovered after the Li_2O/Li electrode was retracted. Some wrinkles on the ribbon were seen (marked by the green arrows in Fig. 3h), indicating possible local plastic deformation accompanying the elastic recovery. Such mechanical manipulation was conducted on many lithiated GNRs and the elastic recovery was reproducible even in multiple compression/release cycles (Fig. 4). Plastic deformation usually occurred to a low extent; however, there were a few cases that the lithiated GNR did not recover the original shape (Fig. 5). The GNR in Fig. 5j formed sharp kink after multiple compressions, indicating that plastic deformation occurred. Importantly, the GNRs never fractured after lithiation and mechanical manipulation, which was in contrast to the MWCNTs under similar loading conditions showing lithiation-induced embrittlement [12].

3.3. *Lack of "geometrical embrittlement" effect in GNRs*

To understand the mechanical robustness of graphene after lithiation, we conducted *ab initio* simulations of graphene and graphite under tension using the Vienna *Ab Initio* Simulation Package (VASP) [24,25]. Procedures of calculations are included in the Experimental and Modeling Details section. Fig. 6a shows the tensile stress–strain curves for the pristine graphene, C_6Li graphene, and C_6Li graphite in the zigzag and the armchair directions. The ideal tensile strength of the pristine graphene is 112 GPa at 20% strain and 121 GPa at 24% strain for the zigzag and the armchair tensile direction, respectively. When Li is added, they are decreased to 98 GPa (zigzag) and 109 GPa (armchair). The effect of lithiation is illustrated by the electron density difference map in Fig. 6b, and the red and the blue isosurfaces indicate the change of

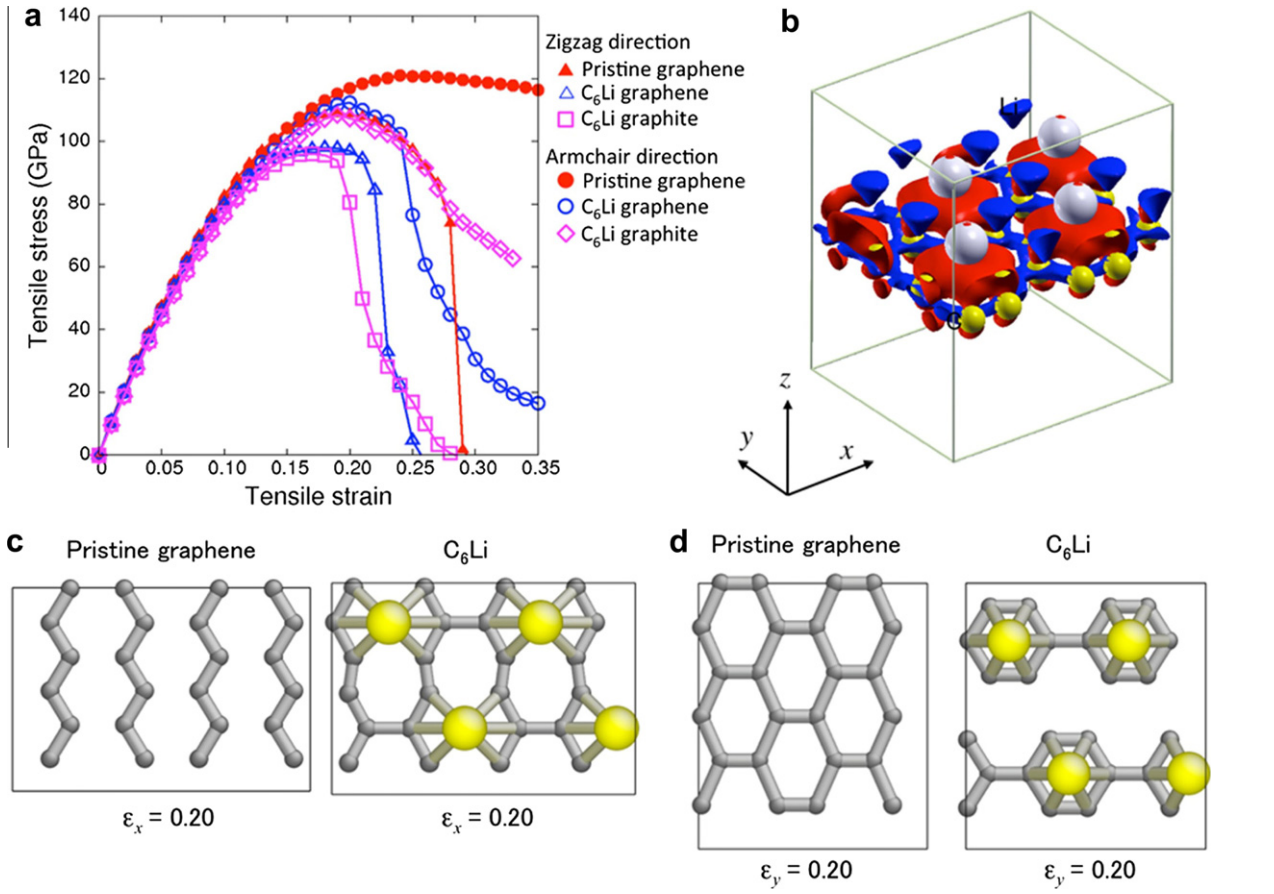

Fig. 6 – Simulations showing the mechanical robustness of graphene in comparison with graphite. (a) Stress–strain curve of the pristine graphene, C_6Li graphene, and C_6Li graphite in armchair and zigzag directions. The lithiated graphene shows almost identical strength as lithiated graphite in both the zigzag and armchair directions. (b) Change in charge density distribution due to lithiation of the graphene. The red and the blue isosurfaces indicate the density change of +0.010 and −0.010 e/Å^3, respectively. (c) Atom configurations of the pristine graphene (left) and C_6Li (right) under tension in zigzag direction at $\varepsilon = 0.20$. (d) Atom configurations of the pristine graphene (left) and C_6Li (right) under tension in armchair direction at $\varepsilon = 0.20$. Large and small spheres in the figure indicate Li and C atoms, respectively.

+0.010 and −0.010 e/Å^3, respectively, relative to the pristine graphene. The electrons are concentrated between the Li and the first neighbor C atoms, and as a result the electron density is reduced at the in-plane C–C bonds. However, this effect of charge transfer is considered to be small on the strong in-plane C–C covalent bonding in graphene because the reduction of the strength from the lithiation is limited to ~10%.

Fig 6c shows the atomic configuration of a pristine graphene and a lithiated C_6Li graphene at 20% strain applied in the zigzag direction. The pristine graphene shows the uniform stretching and breaking of the C–C bonds along the tensile direction. In contrast, the bond deformations are non-uniform in the lithiated graphene because of the charge density shift toward the Li atoms. However, they both fracture by breaking the C–C bonds parallel to the tensile direction and the fracture strains are almost identical. In the case of tension in the armchair direction (Fig. 6d), the pristine graphene accommodated the applied strain by both bond stretch and rotation. The insertion of Li prevented the bond rotation and increased the bond stretch. This caused the 20% reduction of the fracture strain of the lithiated graphene compared to that of the pristine one. The result of the lithiated bulk graphite, which represented the infinite stack of graphene layers, showed almost the same fracture stress and strain as the lithiated graphene. This indicates that the interlayer interaction is negligible in the graphite and the number of the graphite layers has little effect on the strength reduction upon lithiation.

On the other hand, our previous quantum chemical calculations showed that lithiation of a perfect MWCNT can lead to ~50% decrease of its tensile strain to fracture [12]. Compared to the GNRs, such a large reduction of fracture strain in MWCNT is striking, as the basic constituent of both MWCNT and GNRs is graphene, and at a crude level the Li–C chemistry should not be able to tell them apart either. We attribute this striking difference in the potency of Li embrittlement to cylindrical confinement of the MWCNT. In GNRs, the lithiation-induced interlayer expansion causes little in-plane stress, since such expansion can be entirely accommodated by free vertical breathing of the stacked planar graphene layers, as they are weakly constrained in the stacking direction. This is not

the case for MWCNTs, however, since lithiation-induced intertubular expansion (~6% measured in TEM experiments [12]) must be accompanied by a large hoop stress, due to the geometrical requirement of maintaining a circumferentially-closed circle, lithiated or not. This tensile hoop stress was estimated to be ~50 GPa in lithiated MWCNT [12], sufficient to cause local weakening and possibly microcracking of the tube walls.

In cylindrical nanotubes the out-of-plane bending and in-plane stretching are strongly coupled. When the longitudinal tensile load is applied, the MWCNT will contract radially due to Poisson's effect on the circumferentially-closed tube walls, causing a decrease of intertubular spacing. As a result, the intertubular Li is squeezed by the tube walls and it, in turn, acts as a point force to push against them, and thus causes local bending and stretching of the tubes. For example, at an axial strain of 15%, the C–C bond near an intertubular Li is elongated to 1.59 Å, as opposed to 1.54 Å in the pristine counterpart [12]. This additional bond stretch increases with the applied load so as to lower the strain needed to fracture the MWCNT. This local "point force" effect arises naturally in the circumferentially-closed cylindrical tubes, thus leading to severe embrittlement of lithiated MWCNTs. In contrast, it becomes insignificant in the flat and topologically unconstrained graphene and graphite system which have no reason to have significant Poisson's contraction in the vertical stacking direction when subjected to in-plane stretching.

Our experiments and calculations definitively show that Li intercalation severely embrittles MWCNTs, but paradoxically not the GNRs. Based on the explanations above, we see that this embrittlement primarily has a geometrical (or mechanical) origin, instead of a chemical origin. We designate such weakening as "geometrical embrittlement" effect.

4. Conclusion

In summary, lithiation of the GNRs from longitudinally split MWCNTs was studied with *in situ* TEM experiments. Similar to that seen in carbon nanotubes, a Li_2O layer formed on the surface of the GNR stacks during lithiation, accompanying the interlayer expansion of the graphene sheets from 3.4 spacing to 3.6 Å induced by lithium intercalation. The Li_2O layer cannot be completely removed in the delithiation process, indicating possible formation of a stable SEI layer on graphene. Unlike the lithiation-induced embrittlement in the MWCNTs, the graphene nanoribbons showed great flexibility upon mechanical loading and never fractured, consistent with the modeling showing essentially the same strength of lithiated graphene as in lithiated graphite. These results indicate that the mechanically robust graphene with its enormous surface area is indeed a superior material for lithium batteries, either as an active material or as a stable scaffold.

Acknowledgements

Portions of this work were supported by a Laboratory Directed Research and Development (LDRD) project at Sandia National Laboratories (SNL) and partly by Nanostructures for Electrical Energy Storage (NEES), an Energy Frontier Research Center (EFRC) funded by the U.S. Department of Energy, Office of Science, Office of Basic Energy Sciences under Award Number DESC0001160. The LDRD supported the development and fabrication of platforms. The NEES center supported the development of TEM techniques. The Sandia-Los Alamos Center for Integrated Nanotechnologies (CINT) supported the TEM capability. Sandia National Laboratories is a multiprogram laboratory managed and operated by Sandia Corporation, a wholly owned subsidiary of Lockheed Martin Company, for the U.S. Department of Energy's National Nuclear Security Administration under Contract DE-AC04-94AL85000. T.Z. acknowledges support by NSF CMMI-0758554 and 1100205. A.K. and J.L. acknowledge support by NSF CMMI-0728069, DMR-1008104, DMR-1120901 and AFOSR FA9550-08-1-0325. The work at Rice University was supported by Sandia National Laboratory (1100745), funded by the Air Force Office of Scientific Research (FA9550-09-1-0581) and the ONR MURI graphene program (00006766, N00014-09-1-1066). S.Z. acknowledges support by NSF grant CMMI-0900692.

Appendix A. Supplementary data

Supplementary data associated with this article can be found, in the online version, at http://dx.doi.org/10.1016/j.carbon.2012.04.025.

REFERENCES

[1] Novoselov KS, Geim AK, Morozov SV, Jiang D, Zhang Y, Dubonos SV, et al. Electric field effect in atomically thin carbon films. Science 2004;306(5696):666–9.
[2] Sun YQ, Wu QO, Shi GQ. Graphene based new energy materials. Energy Environ Sci 2011;4(4):1113–32.
[3] Park S, Ruoff RS. Chemical methods for the production of graphenes. Nat Nanotechnol 2009;4(4):217–24.
[4] Brownson DAC, Kampouris DK, Banks CE. An overview of graphene in energy production and storage applications. J Power Sources 2011;196(11):4873–85.
[5] Kosynkin DV, Lu W, Sinitskii A, Pera G, Sun Z, Tour JM. Highly conductive graphene nanoribbons by longitudinal splitting of carbon nanotubes using potassium vapor. ACS Nano 2011;5(2):968–74.
[6] Frank IW, Tanenbaum DM, Van der Zande AM, McEuen PL. Mechanical properties of suspended graphene sheets. J Vac Sci Technol, B 2007;25(6):2558–61.
[7] Chou S-L, Wang J-Z, Choucair M, Liu H-K, Stride JA, Dou S-X. Enhanced reversible lithium storage in a nanosize silicon/graphene composite. Electrochem Commun 2010;12(2):303–6.
[8] Wang H, Yang Y, Liang Y, Robinson JT, Li Y, Jackson A, et al. Graphene-wrapped sulfur particles as a rechargeable lithium–sulfur battery cathode material with high capacity and cycling stability. Nano Lett 2011;11(7):2644–7.
[9] Paek S-M, Yoo E, Honma I. Enhanced cyclic performance and lithium storage capacity of SnO_2/graphene nanoporous electrodes with three-dimensionally delaminated flexible structure. Nano Lett 2009;9(1):72–5.
[10] Yoo E, Kim J, Hosono E, Zhou H-s, Kudo T, Honma I. Large reversible Li storage of graphene nanosheet families for use in rechargeable lithium ion batteries. Nano Lett 2008;8(8):2277–82.

[11] Yu MF, Lourie O, Dyer MJ, Moloni K, Kelly TF, Ruoff RS. Strength and breaking mechanism of multiwalled carbon nanotubes under tensile load. Science 2000;287(5453):637–40.
[12] Liu Y, Zheng H, Liu XH, Huang S, Zhu T, Wang J, et al. Lithiation-induced embrittlement of multiwalled carbon nanotubes. ACS Nano 2011;5(9):7245–53.
[13] Masarapu C, Subramanian V, Zhu HW, Wei BQ. Long-cycle electrochemical behavior of multiwall carbon nanotubes synthesized on stainless steel in Li ion batteries. Adv Funct Mater 2009;19(7):1008–14.
[14] Liu XH, Huang JY. In situ tem electrochemistry of anode materials in lithium ion batteries. Energy Environ Sci 2011;4:3844–60.
[15] Liu XH, Zheng H, Zhong L, Huang S, Karki K, Zhang LQ, et al. Anisotropic swelling and fracture of silicon nanowires during lithiation. Nano Lett 2011;11(8):3312–8.
[16] Liu XH, Huang S, Picraux ST, Li J, Zhu T, Huang JY. Reversible nanopore formation in Ge nanowires during lithiation–delithiation cycling: An in situ transmission electron microscopy study. Nano Lett 2011;11(9):3991–7.
[17] Huang JY, Zhong L, Wang CM, Sullivan JP, Xu W, Zhang LQ, et al. In situ observation of the electrochemical lithiation of a single SnO_2 nanowire electrode. Science 2010;330(6010):1515–20.
[18] Liu XH, Zhang LQ, Zhong L, Liu Y, Zheng H, Wang JW, et al. Ultrafast electrochemical lithiation of individual Si nanowire anodes. Nano Lett 2011;11(6):2251–8.
[19] Liu XH, Zhong L, Zhang LQ, Kushima A, Mao SX, Li J, et al. Lithium fiber growth on the anode in a nanowire lithium ion battery during charging. Appl Phys Lett 2011;98(18):183107.
[20] Zhang LQ, Liu XH, Liu Y, Huang S, Zhu T, Gui L, et al. Controlling the lithiation-induced strain and charging rate in nanowire electrodes by coating. ACS Nano 2011;5(6):4800–9.
[21] Ghassemi H, Au M, Chen N, Heiden PA, Yassar RS. In situ electrochemical lithiation/delithiation observation of individual amorphous Si nanorods. ACS Nano 2011;5(10):7805–11.
[22] Ghassemi H, Au M, Chen N, Heiden PA, Yassar RS. Real-time observation of lithium fibers growth inside a nanoscale lithium-ion battery. Appl Phys Lett 2011;99(12):123113.
[23] Wang F, Graetz J, Moreno MS, Ma C, Wu LJ, Volkov V, et al. Chemical distribution and bonding of lithium in intercalated graphite: Identification with optimized electron energy loss spectroscopy. ACS Nano 2011;5(2):1190–7.
[24] Kresse G, Furthmuller J. Efficient iterative schemes for ab initio total-energy calculations using a plane-wave basis set. Phys Rev B 1996;54(16):11169–86.
[25] Kresse G, Hafner J. Ab initio molecular-dynamics for liquid-metals. Phys Rev B 1993;47(1):558–61.
[26] Perdew JP, Wang Y. Accurate and simple analytic representation of the electron-gas correlation-energy. Phys Rev B 1992;45(23):13244–9.
[27] Kresse G, Joubert D. From ultrasoft pseudopotentials to the projector augmented-wave method. Phys Rev B 1999;59(3):1758–75.
[28] Blochl PE. Projector augmented-wave method. Phys Rev B 1994;50(24):17953–79.
[29] Monkhorst HJ, Pack JD. Special points for brillouin-zone interactions. Phys Rev B 1976;13(12):5188–92.
[30] Xu Z, Bando Y, Liu L, Wang WL, Bai XD, Golberg D. Electrical conductivity, chemistry, and bonding alternations under graphene oxide to graphene transition as revealed by in situ TEM. ACS Nano 2011;5(6):4401–6.
[31] Eberlein T, Bangert U, Nair RR, Jones R, Gass M, Bleloch AL, et al. Plasmon spectroscopy of free-standing graphene films. Phys Rev B 2008;77(23):233406.
[32] Hightower A, Ahn CC, Fultz B, Rez P. Electron energy-loss spectrometry on lithiated graphite. Appl Phys Lett 2000;77(2):238–40.